

Calcium and Phosphatidylserine Inhibit Lipid Electropore Formation and Reduce Pore Lifetime

Zachary A. Levine · P. Thomas Vernier

Received: 15 January 2012 / Accepted: 24 June 2012
© Springer Science+Business Media, LLC 2012

Abstract Molecular dynamics simulations of electroporation of homogeneous phospholipid bilayers show that the pore creation time is strongly dependent on the magnitude of the applied electric field. Here, we investigated whether heterogeneous bilayers containing phospholipids with zwitterionic and anionic headgroups exhibit a similar dependence. To facilitate this analysis we divide the life cycle of an electropore into several stages, marking the sequence of steps for pore creation and pore annihilation (restoration of the bilayer after removal of the electric field). We also report simulations of calcium binding isotherms and the effects of calcium ions on the electroporation of heterogeneous lipid bilayers. Calcium binding simulations are consistent with experimental data using a 1:2 Langmuir binding isotherm. We find that calcium ions and phosphatidylserine increase pore creation time and decrease pore annihilation time. For all systems tested, pore creation time was inversely proportional to the bilayer internal electric field.

Keywords Electroporemeabilization · Electroporation · Molecular dynamics · Pore life cycle · Pore creation · Pore annihilation · Calcium · Phosphatidylserine

Introduction

Lipid membranes play many fundamental roles in cell biology, one of which is the partitioning of interior cellular components from the outside world. This barrier function can be disrupted with the application of a sufficiently high external electric field, which permeabilizes the membrane, a process referred to as “electroporemeabilization” or “electroporation” (Hamilton and Sale 1967; Rols and Teissie 1990). Within a few nanoseconds of applying such a field, increases in membrane electrical conductance can be detected (Benz and Zimmermann 1980), and normally impermeant molecules which were previously excluded from the cell are able to penetrate the membrane (Neumann et al. 1982; Rols et al. 1992; Mir et al. 1999). Fluorescent dyes which interact only with intracellular material can be used as indicators of the extent of permeabilization, but the mechanisms and physical structures associated with electroporemeabilization are far from being completely understood and not easily accessible by experiment (Teissie et al. 2005). Since the first reports of reversible and irreversible modifications of membrane conductance by electric fields (Stampfli and Willi 1957; Coster 1965; Hamilton and Sale 1967), steady progress has been made toward a phenomenological understanding of the nature of the permeabilized membrane and the processes that restructure the phospholipid bilayer in an externally applied electric field (Zimmerman et al. 1974; Abidor et al. 1979; Chizmadzhev and Abidor 1980). Observational studies have been enhanced and guided by the development

Z. A. Levine
Department of Physics and Astronomy, Dornsife College
of Letters, Arts & Sciences, University of Southern California,
Los Angeles, CA, USA

Z. A. Levine (✉) · P. T. Vernier
MOSIS, Information Sciences Institute, Viterbi School of
Engineering, University of Southern California, 4676 Admiralty
Way, Marina del Rey, CA 90292, USA
e-mail: zlevine@mosis.com

P. T. Vernier
Ming Hsieh Department of Electrical Engineering,
Viterbi School of Engineering, University of Southern
California, Los Angeles, CA, USA

of continuum electrophysical models of electroporation (Sugar and Neumann 1984; Popescu et al. 1991; Weaver and Chizmadzhev 1996; DeBruin and Krassowska 1998; Neu and Krassowska 1999; Weaver 2003; Vasilkoski et al. 2006), which in turn have contributed to experimental designs and perspectives.

Furthermore, many biological processes are significantly affected by small changes in the local energy landscape, as is the case when an asymmetric distribution of charge is present; thus, a mechanistic understanding of electroporation cannot be restricted to simple, homogeneous lipid bilayer systems. It becomes necessary then to take into account also the effects of inorganic ions which may, for instance, cause membrane lipids to aggregate (Ziegler and Vernier 2008; Boettcher et al. 2011), possibly modifying local surface tensions. Similarly, the behavior of heterogeneous phospholipid bilayers, which may have not only zwitterionic but also anionic and cationic headgroups, must be considered since these additions further perturb the electrochemical landscape and greatly increase the required complexity of analytical models.

Recent advances in high-performance computing have enhanced studies of electroporation using molecular dynamics (MD) simulations of phospholipid bilayers. These simulations suggest that electroporation results at least in part from the formation of discrete, nanoscale electropores that develop in a characteristic sequence: (1) appearance of an electric field-driven water column across the bilayer interior, a process dominated by the energy minimization of interfacial water molecules under an applied electric field (Tieleman 2004; Ziegler and Vernier 2008); (2) construction of a bridge of hydrophilic lipid headgroups and additional hydrating water molecules; and (3) expansion of the pore while the external field continues to be applied (Tieleman et al. 2003; Tieleman 2004; Tarek 2005; Bockmann et al. 2008). Previously, we proposed definitions for these individual stages in pore formation, which we called “pore initiation,” “pore construction” and “pore maturation,” respectively (Levine and Vernier 2010). In this article we refine the nomenclature for these steps.

We have also observed that homogeneous, zwitterionic (containing phosphatidylcholine [PC]) bilayers with varying degrees of hydrocarbon saturation require different “minimum” external electric fields to form pores within a finite period of time (Ziegler and Vernier 2008), which indicates, not surprisingly, that pore formation is affected by lipid properties. Because anionic lipids such as phosphatidylserine (PS) can form complexes in the presence of calcium ions (Vernier et al. 2009), it is reasonable to expect that the incorporation of PS into phospholipid bilayers and the inclusion of Ca^{2+} in the system will also affect pore formation and annihilation. We present here a description

of the electropore life cycles of PC:PS bilayers with and without calcium, extending the analysis we developed for homogeneous PC bilayers (Levine and Vernier 2010).

MD simulations of electroporation must be verified by alignment with existing continuum theories (Weaver and Chizmadzhev 1996) and experiments (Sinn et al. 2006). For validating MD representations of calcium binding to phospholipid bilayers, stoichiometric or coordination complex measurements have been used as a metric (Bockmann and Grubmüller 2004; Vernier et al. 2009; Porasso and Cascales 2009). Here, we propose using binding isotherms as an additional metric to describe the concentration of adsorbed ions at an interface relative to the total ion concentration. At low calcium concentrations one would expect to see linear 1:1 binding, implying that every added calcium ion binds to the interface. At higher calcium concentrations, however, one expects to observe a Langmuir binding isotherm, which is characterized by a transition from linear ion binding to a fixed amount of ion binding when the interface becomes saturated, as others have reported (Bockmann and Grubmüller 2004; Sinn et al. 2006). We compare our simulated calcium binding isotherms with existing experimental and theoretical binding constants for PC:PS bilayers and Ca^{2+} .

Materials and Methods

Simulation Conditions

All simulations were performed using the GROMACS set of programs, version 4.0.5 (Hess et al. 2008), on the University of Southern California High Performance Computing and Communications Linux cluster (<http://www.usc.edu/hpcc/>). Lipid topologies were derived from OPLS united-atom parameters (Berger et al. 1997), and the simple point charge water model was implemented (Berendsen et al. 1981). Each system was coupled to a temperature bath at 310 K with a relaxation time of 0.1 ps and a pressure bath at 1 bar with a relaxation time of 1 ps, each using a weak coupling algorithm (Berendsen et al. 1984). Pressure was coupled semi-isotropically (using a compressibility of $4.5 \times 10^{-5} \text{ bar}^{-1}$) normal to and in the plane of the membrane. Bond lengths were constrained using the LINCS algorithm (Hess et al. 1997) for lipids and SETTLE (Miyamoto and Kollman, 1992) for water. Short-range electrostatic and Lennard-Jones interactions were cut off at 1.0 nm. Long-range electrostatics were calculated by the PME algorithm (Essmann et al. 1995) using fast Fourier transforms and conductive boundary conditions. Reciprocal-space interactions were evaluated on a 0.12-nm grid with fourth-order B-spline interpolation. Periodic boundary conditions were employed to mitigate system size effects.

Systems and Structures

All systems contain a total of 128 lipids—either 1-palmitoyl-2-oleoyl-*sn*-glycero-3-phosphatidylcholine (POPC) or 1-palmitoyl-2-oleoyl-*sn*-glycero-3-phosphatidylserine (POPS)—and about 9,000 water molecules (~ 70 waters/lipid), which resulted in an initial system box size of approximately $7 \times 7 \times 10$ nm. Homogeneous bilayers consist only of POPC. Heterogeneous bilayers were obtained by replacing 20 POPC molecules on a single leaflet with 20 (anionic) POPS molecules and 20 sodium counterions in the bulk water, followed by equilibration until the total area per lipid became constant. Simulations with multiple trials were run in parallel, starting from the same initial positions. To ensure that each trial was independent, every atom was assigned a randomized velocity with a Maxwell distribution at the beginning of the simulation (a built-in function of GROMACS). All systems were equilibrated for a constant area per lipid. Pore creation times were measured for three values of applied external electric field—400, 500 and 600 MV/m—with three independent trials at each electric field strength. Note that 600 MV/m in vacuum corresponds to an effective electric field in aqueous media of about 8 MV/m due to their relative dielectric permittivities. Following pore formation, the external field was removed from a randomly selected simulation, and three independent trials were run to track the annihilation of that single pore. Additionally, we extracted calcium binding coefficients and pore creation times in the presence of calcium from systems where the GROMACS function “genion” was used to replace bulk water molecules with one calcium ion and two chloride counterions. Calcium binding coefficients were extracted after 150 ns, to allow the system to reach equilibrium after calcium addition. Binding coefficients were determined using a 1:2 Langmuir isotherm. Pore radius measurements were obtained by first identifying a pore axis which passes directly through the pore in the z dimension (based on perpendicular x and y water density profiles). Then, bins were assigned between mean lipid phosphorus planes where, for each bin, maximally distant water molecules were identified relative to the pore axis in x and y to obtain local semimajor and semiminor pore diameters. Following this, the semimajor and semiminor pore diameters were averaged together in each bin, and finally all local pore diameters were averaged together to obtain an average pore diameter or pore radius. Pore creation times for systems with calcium present were observed after an electric field was applied to the equilibrated system.

Electropore Life Cycle

The life cycle of an electropore can be divided broadly into a pore creation step and a pore annihilation step, as

described previously (Levine and Vernier 2010). Pore creation (Fig. 1) consists of three stages: initiation, construction and expansion (defined below). Pore annihilation begins when the external electric field is removed from an expanded pore and proceeds through settling, stabilization, deconstruction and dissolution.

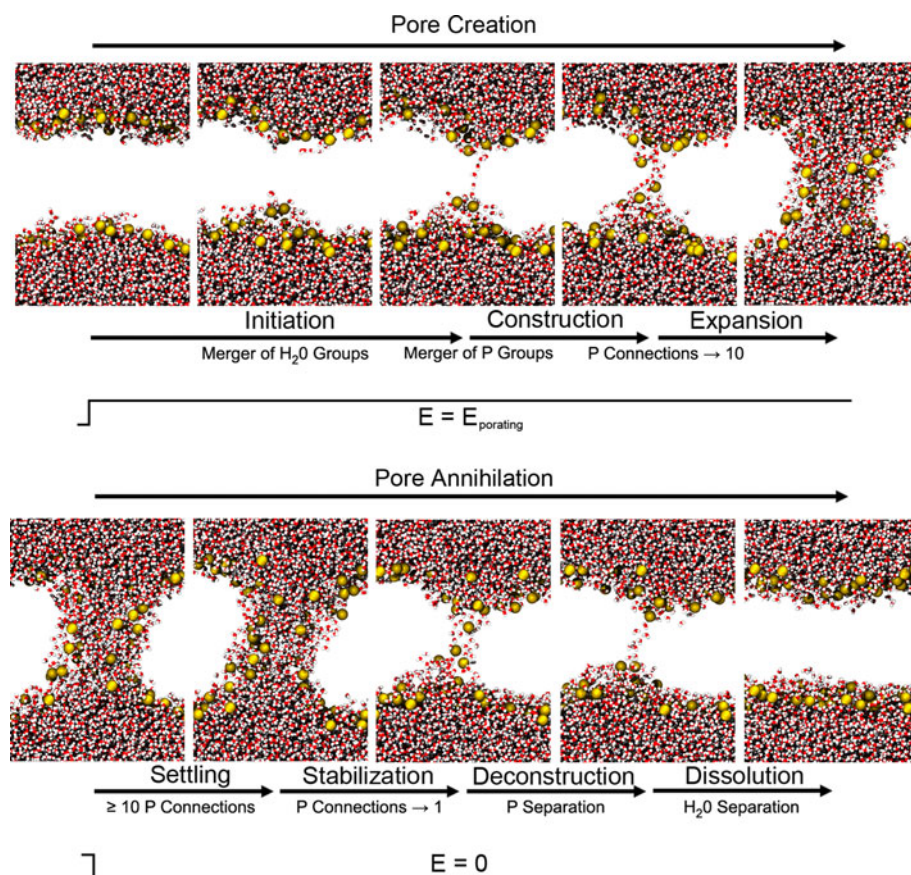
Pore Creation

Pore initiation begins with the application of an external electric field and ends when the two groups of water molecules initially separated by the bilayer merge to become a single group (nonzero water density in every 0.1-nm slice between the two mean planes of phosphorus atoms). In some simulations the combined water groups split again <400 ps after the joining. These transient events are not counted as mergers. Pore construction begins with formation of the membrane-spanning water column (hydrophobic pore [Abidor et al. 1979]), which marks the merger of the water groups and ends when the phosphorus groups that are initially found on the two leaflets of the bilayer follow the water into the membrane interior and merge into a single phosphorus group. (A phosphorus group is defined as a set of atoms, each separated by a maximum distance of 1.2 nm [Sengupta et al. 2008].) Because water and the charged phospholipid headgroups now bridge the membrane interior, this structure is comparable to what is sometimes called a hydrophilic pore (Weaver and Mintzer 1981; Glaser et al. 1988; Leontiadou et al. 2004). Continued application of the porating electric field results in an evolution, or expansion, of the hydrophilic pore. We define an expanded pore arbitrarily as a hydrophilic pore in which at least 10 phosphorus atoms from the initial anodic leaflet are found within 1.2 nm of phosphorus atoms from the cathodic leaflet.

Pore Annihilation

Pore settling, the first stage of pore annihilation, is the quasi-stable period after the field is removed during which the number of anode-to-cathode phosphorus connections fluctuates around the expanded pore criterion (10 connections). Pore stabilization begins when the number of anode-to-cathode phosphorus connections drops below 10 and ends when there is only one anode-to-cathode phosphorus connection. The pore radius decreases around this time to a minimum, about 0.4–0.6 nm. We note that these so-called minimal pores remain hydrophilic and facilitate the conduction of sodium ions when very small external electric fields remain, consistent with theoretical models such as the asymptotic model of electroporation (Neu and Krassowska 1999) which also identify a minimum hydrophilic pore radius of about 0.5 nm. Pore deconstruction, another quasi-stable period, terminates when the single phosphorus group

Fig. 1 Phospholipid electropore life cycle. Structurally distinct steps in pore creation and annihilation as observed in molecular dynamics simulations. Details in “Materials and Methods” section



of the porated bilayer splits into two groups, which remain separate for the remainder of the simulation. At the end of pore deconstruction only the water column remains. We call the disassembly of the water column “pore dissolution.”

Individual pore life cycle times were calculated using a custom Perl program, which codifies the stage boundaries described above. The average value of the electric field at the bilayer midplane (membrane internal electric field) was extracted using the GROMACS function “g potential” over the period from 100 ps after the external electric field was applied to 100 ps before pore construction began. As in our previous work, “internal electric field” was used as a normalizing term (Levine and Vernier 2010).

Images

Molecular graphics images were generated with visual MD (Humphrey et al. 1996).

Results

A complete summary of the pore life cycle results reported here can be found in Figs. 2 and 3 and in Tables 1, 2, 3, 4, 5, 6, 7 and 8. Details are described below.

Pore Creation—Pure POPC and POPC:POPS

At smaller external electric fields, POPC:POPS bilayers have pore creation times that are, on average, slightly longer than homogeneous POPC bilayers (Fig. 2), primarily because of an increase in the pore initiation time, the time it takes water to bridge the membrane interior. The area per lipid, which is strongly correlated with membrane permeability (Mathai et al. 2007), in POPC:POPS systems was about 0.60 compared to 0.66 nm² for POPC bilayers. At higher applied electric fields the differences in pore creation time become minimal and mixed bilayers have pore creation times which are not significantly different from those for homogenous bilayers. Pore initiation times for POPC:POPS are inversely related to the externally applied electric field, and pore construction times remain constant over all electric fields sampled, similar to what we previously reported for homogeneous POPC bilayers (Levine and Vernier 2010). Pore expansion times decrease slightly as higher external electric fields are applied.

Pore Creation—Calcium and POPC

POPC bilayer systems containing calcium ions have, at small external electric fields, pore creation times which are

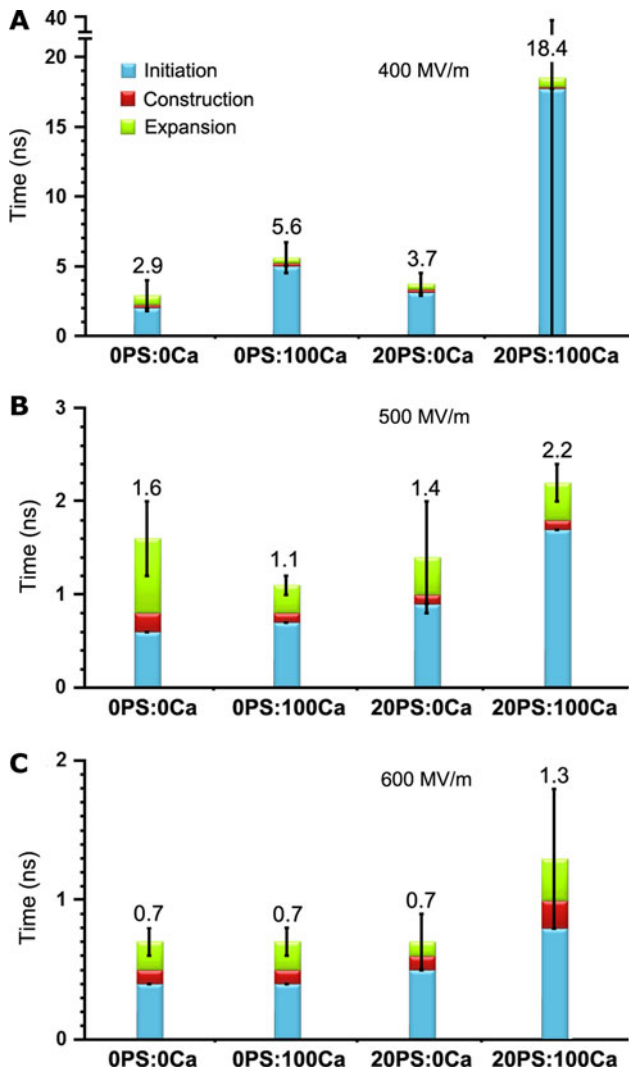


Fig. 2 Pore creation times for three different porating electric fields (400, 500, 600 MV/m) for bilayers consisting of 128 POPC (OPS:0Ca), 128 POPC saturated with calcium (OPS:100Ca), 108 POPC and 20 POPS on a single leaflet without calcium present (20PS:0Ca), and bilayers containing both PS and Ca²⁺ (20PS:100Ca). Systems containing 20 PS also contain 20 Na⁺ as counter ions, and systems containing Ca²⁺ contain two chloride counter ions for every calcium ion. Systems which contain both PS and Ca²⁺ have both sodium and chloride counter ions present. Ca²⁺ and POPS in the bilayer increase the pore initiation time

about twice as long as systems without calcium and about one and a half times as long as those in mixed (POPC:-POPS) bilayers (Fig. 2). As with systems containing PS, when the external electric field is increased, pore creation times of pure POPC systems with calcium and those without calcium are not significantly different. The convergent area per lipid of POPC bilayers with calcium is about 0.56 nm², a value significantly smaller than the area per lipid without calcium reported above. Again, as with systems containing PS, we observed an inverse relationship between externally applied electric field and pore initiation

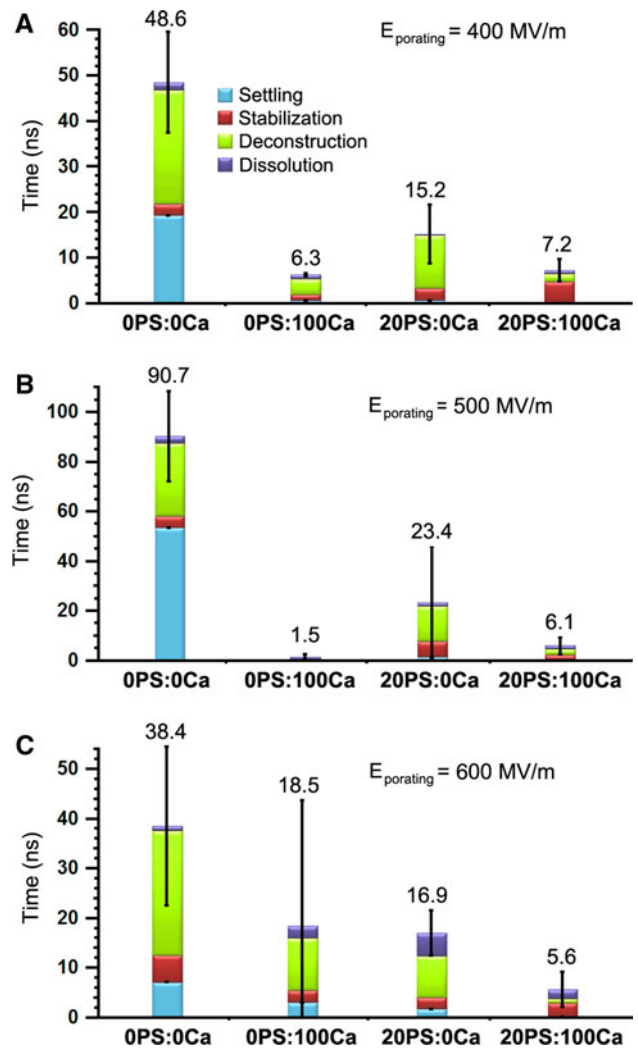


Fig. 3 Pore annihilation times after pore formation in the same systems shown in Fig. 2. Ca²⁺ and POPS in the bilayer decrease the pore annihilation time

time and pore expansion time for POPC bilayer systems containing calcium. Pore construction times remain constant at all electric fields applied.

Pore Creation—Calcium and POPC:POPS

POPC:POPS bilayers containing calcium have pore creation times which are significantly longer than those for pure POPC systems, with or without calcium, and longer than POPC:-POPS systems without calcium (Fig. 2). This is true for all electric fields applied, even very high fields where for all of the systems described above the pore creation times were not significantly different. The average area per lipid of POPC:-POPS bilayers with calcium was about 0.55 nm² before a field was applied, slightly smaller than the area per lipid of POPC bilayers with calcium. As with all other systems reported here, both pore initiation times and pore expansion times decrease

Table 1 POPC pore creation times without PS and without Ca²⁺ Levine and Vernier (2010)

Applied field (MV/m)	Average internal field (MV/m)	Initiation		Construction		Expansion		Creation	
		Time (ns)	Mean (ns)	Time (ns)	Mean (ns)	Time (ns)	Mean (ns)	Time (ns)	Mean (ns)
400	1,630	2.8		0.0		0.5		3.3	
		2.3	2.0 ± 1.0	0.3	0.2 ± 0.2	1.1	0.8 ± 0.3	3.7	2.9 ± 1.1
		0.8		0.2		0.7		1.7	
500	2,180	0.9		0.1		1.0		2.0	
		0.6	0.6 ± 0.3	0.2	0.2 ± 0.1	0.5	0.8 ± 0.3	1.3	1.6 ± 0.4
		0.4		0.3		0.9		1.6	
600	2,347	0.5		0.1		0.1		0.7	
		0.5	0.4 ± 0.2	0.0	0.1 ± 0.1	0.3	0.2 ± 0.1	0.8	0.7 ± 0.1
		0.2		0.2		0.2		0.6	

Table 2 POPC pore creation times without PS and with 100 Ca²⁺

Applied field (MV/m)	Average internal field (MV/m)	Initiation		Construction		Expansion		Creation	
		Time (ns)	Mean (ns)	Time (ns)	Mean (ns)	Time (ns)	Mean (ns)	Time (ns)	Mean (ns)
400	1,373	6.2		0.1		0.5		6.8	
		4.6	5.0 ± 1.0	0.1	0.2 ± 0.1	0.4	0.4 ± 0.2	5.1	5.6 ± 1.1
		4.3		0.3		0.2		4.8	
500	1,837	0.9		0.1		0.2		1.2	
		0.8	0.8 ± 0.2	0.1	0.1 ± 0.0	0.2	0.3 ± 0.1	1.1	1.1 ± 0.1
		0.6		0.1		0.4		1.1	
600	2,292	0.4		0.2		0.2		0.8	
		0.4	0.4 ± 0.0	0.1	0.1 ± 0.1	0.2	0.2 ± 0.0	0.7	0.7 ± 0.1
		0.4		0.1		0.2		0.7	

Table 3 POPC pore creation times with PS and without Ca²⁺

Applied field (MV/m)	Average internal field (MV/m)	Initiation		Construction		Expansion		Creation	
		Time (ns)	Mean (ns)	Time (ns)	Mean (ns)	Time (ns)	Mean (ns)	Time (ns)	Mean (ns)
400	1,707	2.2		0.3		0.4		2.9	
		3.2	3.1 ± 0.9	0.1	0.2 ± 0.1	0.4	0.4 ± 0.0	3.7	3.7 ± 0.8
		3.9		0.2		0.4		4.5	
500	1,930	0.5		0.2		0.2		0.9	
		1.4	0.9 ± 0.5	0.1	0.1 ± 0.1	0.5	0.4 ± 0.2	2.0	1.4 ± 0.6
		0.9		0.1		0.4		1.4	
600	2,197	0.2		0.2		0.2		0.6	
		0.3	0.4 ± 0.3	0.1	0.1 ± 0.1	0.1	0.1 ± 0.1	0.5	0.7 ± 0.2
		0.7		0.1		0.1		0.9	

as the external electric field increases, while pore construction times are similar for all values of electric field applied in these simulations.

Pore Annihilation—Pure POPC and POPC:POPS

POPC:POPS bilayers have pore annihilation times about three times smaller than pure POPC bilayers (Fig. 3). All

pore annihilation stages except stabilization are shortened relative to pure POPC, and this is true regardless of the value of the electric field used to create the pore. The average pore radius at the start of the annihilation step was about 2.3 nm for POPC:POPS systems, similar to the average pore radius for pure PC bilayers, 2.2 nm. Also, pure POPC bilayer pore annihilation times are dominated by pore settling and pore deconstruction.

Table 4 POPC pore creation times with PS and with 100 Ca²⁺

Applied field (MV/m)	Average internal field (MV/m)	Initiation		Construction		Expansion		Creation	
		Time (ns)	Mean (ns)	Time (ns)	Mean (ns)	Time (ns)	Mean (ns)	Time (ns)	Mean (ns)
400	1,417	8.9		0.0		0.6		9.5	
		5.1	17.7 ± 18.6	0.1	0.1 ± 0.1	0.9	0.7 ± 0.2	6.0	18.4 ± 18.5
		39.0		0.0		0.6		39.6	
500	1,833	1.5		0.1		0.3		1.9	
		1.8	1.7 ± 0.1	0.2	0.1 ± 0.1	0.3	0.4 ± 0.1	2.3	2.2 ± 0.2
		1.7		0.1		0.5		2.3	
600	2,230	1.0		0.4		0.4		1.8	
		0.8	0.9 ± 0.1	0.0	0.2 ± 0.2	0.1	0.3 ± 0.2	0.9	1.3 ± 0.5
		0.8		0.1		0.3		1.2	

Table 5 POPC pore annihilation times without PS and without Ca²⁺ Levine and Vernier (2010)

Field During Poration (MV/m)	Settling		Stabilization		Deconstruction		Dissolution		Annihilation	
	Time (ns)	Mean (ns)	Time (ns)	Mean (ns)	Time (ns)	Mean (ns)	Time (ns)	Mean (ns)	Time (ns)	Mean (ns)
400	7.3		3.0		24.6		2.9		37.8	
	29.2	19.4 ± 11.1	3.7	2.5 ± 1.5	25.9	25.0 ± 0.8	1.1	1.7 ± 1.0	59.9	48.6 ± 11.1
	21.6		0.8		24.6		1.1		48.1	
500	84.4		7.5		17.3		1.4		110.6	
	17.3	53.7 ± 33.9	4.0	4.7 ± 2.5	49.8	29.3 ± 17.8	4.2	2.9 ± 1.4	75.3	90.7 ± 18.1
	59.5		2.7		20.9		3.0		86.1	
600	11.4		1.0		8.1		1.5		22.0	
	3.8	7.1 ± 3.9	6.4	5.4 ± 4.0	28.5	25.1 ± 15.5	0.7	0.9 ± 0.6	39.4	38.4 ± 16.0
	6.2		8.7		38.6		0.4		53.9	

Table 6 POPC pore annihilation times without PS and with 100 Ca²⁺

Field during poration (MV/m)	Settling		Stabilization		Deconstruction		Dissolution		Annihilation	
	Time (ns)	Mean (ns)	Time (ns)	Mean (ns)	Time (ns)	Mean (ns)	Time (ns)	Mean (ns)	Time (ns)	Mean (ns)
400	0.0		0.4		4.6		1.0		6.0	
	0.0	0.6 ± 1.0	2.3	1.4 ± 1.0	3.3	3.3 ± 1.3	0.7	1.0 ± 0.3	6.3	6.3 ± 0.3
	1.7		1.6		2.1		1.2		6.6	
500	0.1		0.1		1.2		0.5		1.9	
	0.0	0.1 ± 0.1	0.1	0.1 ± 0.0	0.1	0.5 ± 0.6	0.2	0.9 ± 0.9	0.4	1.5 ± 0.9
	0.0		0.1		0.1		1.9		2.1	
600	0.0		0.5		2.3		2.7		5.5	
	9.0	3.0 ± 5.2	5.4	2.4 ± 2.6	28.8	10.6 ± 15.8	4.4	2.4 ± 2.1	47.6	18.5 ± 25.3
	0.0		1.3		0.8		0.2		2.3	

POPC:POPS bilayers exhibit very short pore settling times and significantly reduced pore deconstruction times compared to POPC systems, reducing the overall time required to annihilate POPC:POPS electropores. An initial decrease in pore radius occurs immediately after the

field is removed in both POPC and POPC:POPS bilayers, from about 2.3 to about 0.5 nm over the first few nanoseconds. This initial reduction of the pore radius does not appear to be correlated with pore settling time (Fig. 4).

Table 7 POPC pore annihilation times with PS and without Ca²⁺

Field during poration (MV/m)	Settling		Stabilization		Deconstruction		Dissolution		Annihilation	
	Time (ns)	Mean (ns)	Time (ns)	Mean (ns)	Time (ns)	Mean (ns)	Time (ns)	Mean (ns)	Time (ns)	Mean (ns)
400	0.8		2.8		4.9		0.1		8.6	
	0.3	0.6 ± 0.3	3.7	2.7 ± 1.1	16.7	11.6 ± 6.0	0.7	0.3 ± 0.3	21.4	15.2 ± 6.4
	0.8		1.6		13.1		0.1		15.6	
	3.2		0.6		2.4		3.1		9.3	
500	0.9	1.5 ± 1.5	1.8	6.1 ± 8.5	8.7	14.2 ± 15.3	0.1	1.6 ± 1.5	11.5	23.4 ± 22.5
	0.3		15.9		31.4		1.7		49.3	
	1.1		1.5		13.8		3.6		20.0	
600	1.0	1.7 ± 1.1	1.2	2.3 ± 1.7	7.2	8.3 ± 5.1	9.5	4.7 ± 4.4	18.9	16.9 ± 4.5
	2.9		4.2		3.8		0.9		11.8	

Table 8 POPC pore annihilation times with PS and with 100 Ca²⁺

Field during poration (MV/m)	Settling		Stabilization		Deconstruction		Dissolution		Annihilation	
	Time (ns)	Mean (ns)	Time (ns)	Mean (ns)	Time (ns)	Mean (ns)	Time (ns)	Mean (ns)	Time (ns)	Mean (ns)
400	0.0		7.1		2.5		0.2		9.8	
	0.1	0.1 ± 0.1	2.3	4.7 ± 2.4	2.0	1.7 ± 1.0	0.6	0.8 ± 0.7	5.0	7.2 ± 2.4
	0.0		4.8		0.5		1.5		6.8	
	0.0		1.7		1.5		1.6		4.8	
500	0.1	0.1 ± 0.1	1.9	2.2 ± 0.8	0.4	2.3 ± 2.4	1.0	1.5 ± 0.4	3.4	6.1 ± 3.5
	0.1		3.1		5.0		1.8		10.0	
	0.1		4.5		1.2		3.7		9.5	
600	0.2	0.1 ± 0.1	3.0	2.8 ± 1.8	0.2	0.8 ± 0.5	1.1	1.9 ± 1.6	4.5	5.6 ± 3.5
	0.0		0.9		0.9		0.9		2.7	

Pore Annihilation—Calcium and POPC

Pure POPC systems containing calcium have dramatically reduced pore annihilation times compared to POPC systems without calcium (Fig. 3). For pores created at 400 and 500 MV/m, POPC–Ca²⁺ systems exhibit virtually no pore settling, while all remaining stages take no more than a few nanoseconds to complete. For pores created at 600 MV/m, calcium still significantly reduces the pore annihilation time but the variation from simulation to simulation is large. As with POPC:POPS and pure POPC bilayers without calcium, the pore radius is reduced in POPC systems containing calcium to 0.5 nm after only a few nanoseconds but with calcium present the initial pore radius immediately after the external field is removed is 1.7 nm, about 0.6 nm smaller than the pores in the annihilation simulations without calcium.

Pore Annihilation—Calcium and POPC:POPS

POPC:POPS systems with calcium have pore annihilation times which are also significantly shorter than those for

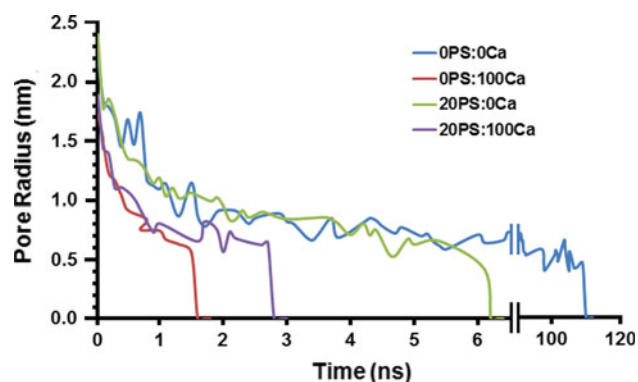


Fig. 4 Evolution of pore radius after removal of the porating electric field for the same systems shown in Fig. 2. This example, from a simulation in which $E_{\text{porating}} = 500$ MV/m, is representative of pore annihilation behavior for all values of E_{porating} examined in this work. Average initial pore radii are 2.2 nm for 0PS:0Ca systems, 2.4 nm for 20PS:0Ca systems, 1.7 nm for 0PS:100Ca systems, and 1.9 nm for 20PS:100Ca systems

pure POPC bilayers and POPC:POPS systems without calcium. POPC:POPS–Ca²⁺ annihilation times are comparable to those for POPC–Ca²⁺ and POPC:POPS (no

calcium) systems. For pores created at the highest electric field, POPC:POPS–Ca²⁺ systems have the shortest pore annihilation times of all systems sampled. Pore settling time for these systems is too short to measure in about half of the trials; the longest settling time measured for POPC:POPS–Ca²⁺ is 200 ps. Stabilization is the dominant step in pore annihilation for these systems, and the variance in pore annihilation time is much smaller than for pure POPC systems without calcium. As with POPC–Ca²⁺ systems, the initial pore radius for POPC:POPS–Ca²⁺ systems after the porating field is removed is about 1.8 nm. As soon as the pore radius decreases to about 0.5 nm in the POPC:POPS–Ca²⁺ systems, the pores dissipate quickly, in contrast with pure POPC bilayers without calcium, where pores remain open with a radius around 0.5 nm for many tens of nanoseconds.

Calcium Binding

To assess the validity of our calcium ion models in POPC:POPS systems, we constructed a binding isotherm (Fig. 5), which plots the amount of bound calcium ions against the bulk calcium ion concentration. Our data can be described by a 1:2 Langmuir binding isotherm between calcium and phospholipid (Altenbach and Seelig 1984) and with binding isotherms taken from experiments with pure and mixed vesicles (Sinn et al. 2006). Additionally, for small calcium concentrations we see linear 1:1 binding. Calcium appears to bind preferentially to PS carboxyl and PC:PS phosphoryl oxygens. From systems equilibrated for 150 ns (Vernier et al. 2009) we extracted a calcium binding coefficient, $K = 2.56 \text{ M}^{-1}$.

Discussion

Electropore Life Cycle for POPC:POPS Bilayers

We have shown that incorporation of the anionic phospholipid POPS into a POPC (zwitterionic) bilayer slightly increases the time required for pore creation at lower external electric fields and drastically decreases the time required for pore annihilation for electropores created at all external electric fields. PS bilayers have a smaller area per lipid (Mukhopadhyay et al. 2004) compared to PC bilayers, and changes in surface tension, which may be affected by locally varying area per lipid, have been shown to affect pore formation (Lewis 2003; Tieleman et al. 2003; Tieleman 2004).

At higher electric fields pore creation times for POPC:POPS bilayers are similar to those for pure POPC bilayers. As previous studies have shown, interfacial water is a dominant component of pore formation (Tieleman

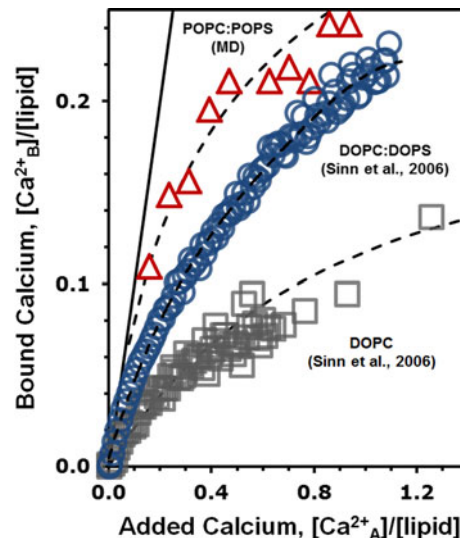


Fig. 5 Calcium binding curves show rough correspondence between experimental and simulated results. The data can be described by a 1:2 Langmuir binding isotherm, consistent with formation of Ca:PS₂ complexes

2004; Tarek 2005; Ziegler and Vernier 2008), and we can speculate that the formation of bilayer-spanning water bridges in the strong interfacial electric field gradients that result from application of large external electric fields is only weakly influenced by PS or PC interactions. This is consistent with the stochastic pore hypothesis for electroporation (Sugar and Neumann 1984; Popescu et al. 1991; Neu and Krassowska 1999; Weaver 2003) and previous observations (Levine and Vernier 2010), in which pore creation time was inversely correlated with the magnitude of the applied electric field. In this scheme our highest external electric field, 600 MV/m, is at or near a saturating value for porating fields for POPC and POPC:POPS bilayers. In this saturation range electropores are created in similar, asymptotically convergent times. We also observe comparable pore radii for POPC:POPS and pure POPC bilayers at the end of the pore creation step, despite small differences in area per lipid, suggesting that the radius of an electropore is only partially dependent on phospholipid areal density.

Effects of Calcium on Pore Life Cycle

Calcium in pure POPC bilayer systems delays pore creation at lower external electric fields and greatly reduces the time required for pore annihilation. POPC:POPS systems containing calcium have even longer pore creation times at lower electric fields. The pore radius after creation is lower in both POPC and POPC:POPS systems containing calcium than for systems without calcium. As indicated above, this may be partially associated with significantly smaller area per lipid values found both experimentally (Mattai et al. 1989) and in

simulations (Bockmann and Grubmüller 2004) when calcium is present.

Even though the area per lipid is similar for POPC–Ca²⁺ and POPC:POPS–Ca²⁺ systems, it has been shown experimentally and in MD simulations that calcium binds with more affinity to PC:PS vesicles than to pure PC vesicles (Sinn et al. 2006; Vernier et al. 2009), forming Ca²⁺–PS complexes involving PS carboxyl and phosphoryl oxygens. By increasing the total number of calcium-lipid complexes, we are effectively decreasing the area per lipid of our system and thus increasing membrane surface tension. Until the molecular-level details of water intrusion and bridge construction across the bilayer have been fully explained, we can only presume that increases in surface tension associated with the presence of Ca²⁺ and PS lead to increases in the energy barrier for interfacial water entry into the bilayer interior and an associated increase in pore creation times. Alternatively, when the external field is removed, a change in surface tension would result in a change in the pore edge tension since the two quantities are related (Ryham et al. 2011); thus, we would expect to see modified pore annihilation times for systems with PS and/or Ca²⁺ present compared to systems without PS and Ca²⁺.

In addition, POPC:POPS–Ca²⁺ systems exhibit very short pore annihilation times (a few nanoseconds), similar to the time scale of pore creation. This is an order of magnitude faster than pure POPC systems, which have pore annihilation times that are tens of nanoseconds or even more than 100 ns in simulations (Levine and Vernier 2010). These timescales are similar to the resealing timescales reported in other MD simulations (Tarek 2005); however, a large discrepancy still exists between simulated pore annihilation times and experimental resealing times, which occur on timescales of milliseconds (Melikov et al. 2001) to hundreds of seconds (Koronkiewicz et al. 2002). These long-lasting pores occur in living cell membranes, not simple phospholipid bilayers, suggesting that some membrane restructuring beyond lipid nanopore formation occurs and that the permeabilizing structures in cell membranes have significantly stabilizing features.

Molecular and Continuum Models of Lipid Electropores

Our results agree (Fig. 6) with numerical models which predict an exponential relationship between transmembrane potential and pore creation (Neu and Krassowska 1999) for all configurations tested. (Note that there is a direct relationship between the internal electric field and the transmembrane potential.) The electric field is the dominant term for pore creation, and although we see variations in pore creation time at smaller fields for POPC versus POPC:POPS or with the introduction of calcium ions, pore creation occurs at similar

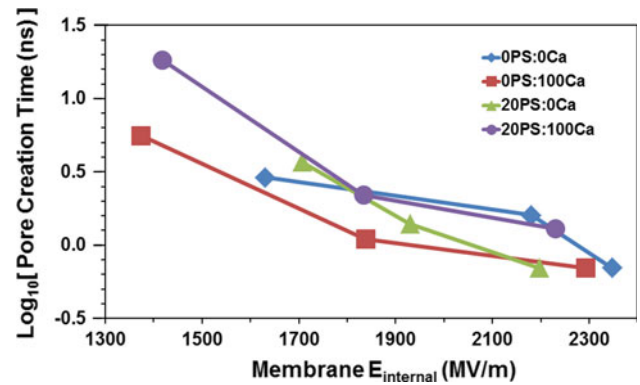


Fig. 6 Lipid electropore creation time as a function of bilayer internal electric field for the systems shown in Fig. 2. The log scale reflects the exponential dependence of the probability of pore formation on the applied electric field. Internal electric field is used here as a normalizing quantity

times for very high electric fields. Pore annihilation is a stochastic process in some models (Weaver and Chizmadzhev 1996), and indeed we see large variances in the pore annihilation time, which suggests that local fluctuations and dynamics strongly influence restructuring of the bilayer.

Our simulations of calcium binding to POPC and POPC:POPS bilayers provide support for the validity of the calcium ion model we are using. Our binding isotherm for POPC:POPS bilayers is similar to experimental data for dioleoyl-phosphatidylcholine:phosphatidylserine (DOPC:DOPS) vesicles (Sinn et al. 2006) using a 1:2 Langmuir isotherm. The binding coefficient extracted from our simulations is 2.56 M⁻¹, in the range of the measured value of 13.8 M⁻¹ (Altenbach and Seelig 1984), although experiments at different NaCl and Ca²⁺ concentrations are difficult to compare directly. Better models may lead to increased accuracy in determining proper binding coefficients.

Although our simple, largely intuitive characterization of the stages in the lipid electropore life cycle provides a useful scheme for analysis of pore creation and pore annihilation, a more sophisticated approach will build on this foundation to incorporate systematic measurements of the pore radius and pore energies (Neu and Krassowska 1999) and to include the atomic-scale electric field landscape and the interactions of water oxygen and hydrogen with the electron-dense acyl oxygens deep in the phospholipid bilayer interface. Once these key components of the molecular structure of electropores are accurately represented, the additional complexities of lipid heterogeneity, membrane proteins and cytoskeletal and glycocalyx attachments can be added to the model one by one, until we approach a useful representation of the living cell membrane in a porating electric field.

Acknowledgements We thank Rumiana Dimova for stimulating discussions and insightful input on calcium binding. Computing

resources were provided by the USC Center for High Performance Computing and Communications (<http://www.usc.edu/hpcc/>). This work was made possible in part by the Air Force Office of Scientific Research and by MOSIS, Information Sciences Institute, Viterbi School of Engineering, University of Southern California.

References

- Abidor IG, Arakelyan VB, Chernomordik LV et al (1979) Electric breakdown of bilayer lipid-membranes. 1. Main experimental facts and their qualitative discussion. *Bioelectrochem Bioenerg* 6:37–52
- Altenbach C, Seelig J (1984) Calcium binding to phosphatidylcholine bilayers as studied by deuterium magnetic resonance. Evidence for the formation of a calcium complex with two phospholipid molecules. *Biochemistry* 23(17):3913–3920
- Benz R, Zimmermann U (1980) Pulse-length dependence of the electrical breakdown in lipid bilayer-membranes. *Biochim Biophys Acta* 597:637–642
- Berendsen HJC, Postma JPM, van Gunsteren WF et al (1981) Interaction models for water in relation to protein hydration. In: Pullman B (ed) *Intermolecular forces*. Reidel, Dordrecht, pp 331–342
- Berendsen HJC, Postma JPM, van Gunsteren WF et al (1984) Molecular-dynamics with coupling to an external bath. *J Chem Phys* 81:3684–3690
- Berger O, Edholm O, Jahnig F (1997) Molecular dynamics simulations of a fluid bilayer of dipalmitoylphosphatidylcholine at full hydration, constant pressure, and constant temperature. *Biophys J* 72:2002–2013
- Bockmann RA, Grubmuller H (2004) Multistep binding of divalent cations to phospholipid bilayers: a molecular dynamics study. *Angew Chem* 43(8):1021–1024
- Bockmann RA, de Groot BL, Kakorin S et al (2008) Kinetics, statistics, and energetics of lipid membrane electroporation studied by molecular dynamics simulations. *Biophys J* 95:1837–1850
- Boettcher JM, Davis-Harrison RL, Clay MC et al (2011) Atomic view of calcium-induced clustering of phosphatidylserine in mixed lipid bilayers. *Biochemistry* 50:2264–2273
- Chizmadzhev YA, Abidor IG (1980) Bilayer lipid-membranes in strong electric-fields. *Bioelectrochem Bioenerg* 7:83–100
- Coster HGL (1965) A quantitative analysis of voltage-current relationships of fixed charge membranes and associated property of punch-through. *Biophys J* 5:669
- DeBruin KA, Krassowska W (1998) Electroporation and shock-induced transmembrane potential in a cardiac fiber during defibrillation strength shocks. *Ann Biomed Eng* 26:584–596
- Essmann U, Perera L, Berkowitz ML et al (1995) A smooth particle mesh Ewald method. *J Chem Phys* 103:8577–8593
- Glaser RW, Leikin SL, Chernomordik LV et al (1988) Reversible electrical breakdown of lipid bilayers: formation and evolution of pores. *Biochim Biophys Acta* 940:275–287
- Hamilton WA, Sale AJH (1967) Effects of high electric fields on microorganisms. 2. Mechanism of action of lethal effect. *Biochim Biophys Acta* 148:789–800
- Hess B, Bekker H, Berendsen HJC et al (1997) LINCS: a linear constraint solver for molecular simulations. *J Comput Chem* 18:1463–1472
- Hess B, Kutzner C, van der Spoel D et al (2008) GROMACS 4: algorithms for highly efficient, load-balanced, and scalable molecular simulation. *J Chem Theory Comput* 4(3):435–447
- Humphrey W, Dalke A, Schulten K (1996) VMD: visual molecular dynamics. *J Mol Graph* 14:33–38
- Koronkiewicz S, Kalinowski S, Bryl K (2002) Programmable chronopotentiometry as a tool for the study of electroporation and resealing of pores in bilayer lipid membranes. *Biochim Biophys Acta Biomembr* 1561:222–229
- Leontiadou H, Mark AE, Marrink SJ (2004) Molecular dynamics simulations of hydrophilic pores in lipid bilayers. *Biophys J* 86:2156–2164
- Levine ZA, Vernier PT (2010) Life cycle of an electropore: field-dependent and field-independent steps in pore creation and annihilation. *J Membr Biol* 236:27–36
- Lewis TJ (2003) A model for bilayer membrane electroporation based on resultant electromechanical stress. *IEEE Trans Dielect Elect Insul* 10:769–777
- Mathai JC, Tristram-Nagle S, Nagle JF et al (2007) Structural determinants of water permeability through the lipid membrane. *J Gen Physiol* 131:69–76
- Mattai J, Hauser H, Demel RA et al (1989) Interactions of metal ions with phosphatidylserine bilayer membranes: effect of hydrocarbon chain unsaturation. *Biochemistry* 28(5):2322–2330
- Melikov KC, Frolov VA, Shcherbakov A, Samsonov AV, Chizmadzhev YA, Chernomordik LV (2001) Voltage-induced nonconductive pre-pores and metastable single pores in unmodified planar lipid bilayer. *Biophys J* 80:1829–1836
- Mir LM, Bureau MF, Gehl J et al (1999) High-efficiency gene transfer into skeletal muscle mediated by electric pulses. *Proc Natl Acad Sci USA* 96:4262–4267
- Miyamoto S, Kollman PA (1992) Settle: an analytical version of the shake and rattle algorithm for rigid water models. *J Comput Chem* 13:952–962
- Mukhopadhyay P, Monticelli L, Tieleman DP (2004) Molecular dynamics simulation of a palmitoyl-oleoyl phosphatidylserine bilayer with Na⁺ counterions and NaCl. *Biophys J* 86(3):1601–1609
- Neu JC, Krassowska W (1999) Asymptotic model of electroporation. *Phys Rev E* 59:3471–3482
- Neumann E, Schaeferriidder M, Wang Y et al (1982) Gene-transfer into mouse lymphoma cells by electroporation in high electric-fields. *EMBO J* 1:841–845
- Popescu D, Rucareanu C, Victor G (1991) A model for the appearance of statistical pores in membranes due to self oscillations. *Bioelectrochem Bioenerg* 25:91–103
- Porasso RD, Cascales JLL (2009) Study of the effect of Na⁺ and Ca²⁺ ion concentration on the structure of an asymmetric DPPC/DPPC + DPPS lipid bilayer by molecular dynamics simulation. *Colloids Surf B Biointerfaces* 73:42–50
- Rols MP, Teissie J (1990) Electroporation of mammalian cells—quantitative analysis of the phenomenon. *Biophys J* 58:1089–1098
- Rols MP, Coulet D, Teissie J (1992) Highly efficient transfection of mammalian cells by electric-field pulses: application to large volumes of cell culture by using a flow system. *Eur J Biochem* 206:115–121
- Ryham R, Berezovik I, Cohen FS (2011) Aqueous viscosity is the primary source of friction in lipidic pore dynamics. *Biophys J* 101:2929–2938
- Sengupta D, Leontiadou H, Mark AE et al (2008) Toroidal pores formed by antimicrobial peptides show significant disorder. *Biochim Biophys Acta Biomembr* 1778:2308–2317
- Sinn CG, Antonietti M, Dimova R (2006) Binding of calcium to phosphatidylcholine: phosphatidylserine membranes. *Colloids Surf A Physicochem Eng Asp* 282:410–419
- Stampfli R, Willi M (1957) Membrane potential of a ranvier node measured after electrical destruction of its membrane. *Experientia* 13:297–298
- Sugar IP, Neumann E (1984) Stochastic model for electric field-induced membrane pores. *Electroporation. Biophys Chem* 19:211–225

- Tarek M (2005) Membrane electroporation: a molecular dynamics simulation. *Biophys J* 88:4045–4053
- Teissie J, Golzio M, Rols MP (2005) Mechanisms of cell membrane electroporation: a minireview of our present (lack of?) knowledge. *Biochim Biophys Acta* 1724:270–280
- Tieleman DP (2004) The molecular basis of electroporation *BMC Biochem* 5:10
- Tieleman DP, Leontiadou H, Mark AE et al (2003) Simulation of pore formation in lipid bilayers by mechanical stress and electric fields. *J Am Chemical Soc* 125:6382–6383
- Vasilkoski Z, Esser AT, Gowrishankar TR, Weaver JC (2006) Membrane electroporation: the absolute rate equation and nanosecond time scale pore creation. *Phys Rev E* 74:021904
- Vernier PT, Ziegler MJ, Dimova R (2009) Calcium binding and head group dipole angle in phosphatidylserine: phosphatidylcholine bilayers. *Langmuir* 25(2):1020–1027
- Weaver JC (2003) Electroporation of biological membranes from multicellular to nano scales. *IEEE Trans Dielect Elect Insul* 10:754–768
- Weaver JC, Chizmadzhev YA (1996) Theory of electroporation: a review. *Bioelectrochem Bioenerg* 41:135–160
- Weaver JC, Mintzer RA (1981) Decreased bilayer stability due to transmembrane potentials. *Phys Lett A* 86:57–59
- Ziegler MJ, Vernier PT (2008) Interface water dynamics and porating electric fields for phospholipid bilayers. *J Phys Chem B* 112:13588–13596
- Zimmerman U, Pilwat G, Riemann F (1974) Dielectric breakdown of cell membranes. *Biophys J* 14:881–899